Insight into the Binding Properties of MEKK3 PB1 to MEK5 PB1 from Its Solution Structure[†,‡]

Qi Hu, Weiqun Shen, Hongda Huang, Jiangxin Liu, Jiahai Zhang, Xiaojuan Huang, Jihui Wu,* and Yunyu Shi*

Hefei National Laboratory for Physical Sciences at Microscale and School of Life Sciences, University of Science and Technology of China, Hefei, Anhui 230026, People's Republic of China

Received July 7, 2007; Revised Manuscript Received September 12, 2007

ABSTRACT: MEKK3 is a mitogen-activated protein kinase kinase kinase that participates in various signaling pathways. One of its functions is to activate the ERK5 signal pathway by phosphorylating and activating MEK5. MEKK3 and MEK5 each harbors a PB1 domain in the N-terminus, and they form a heterodimer via PB1−PB1 domain interaction that was reported to be indispensable to the activation of MEK5. Using NMR spectroscopy, we show here that a prolyl isomerization of the Gln38−Pro39 bond is present in MEKK3 PB1, which is the first case of structural heterogeneity within PB1 domains. We have solved the solution structures of both isomers and found a major difference between them in the Pro39 region. Residues Gly37−Leu40 form a type VIb β-turn in the cis conformation, whereas no obvious character of β-turn was observed in the trans conformation. Backbone dynamics studies have unraveled internal motions in the β3/β4-turn on a microsecond−millisecond time scale. Further investigation of its binding properties with MEK5 PB1 has demonstrated that MEKK3 PB1 binds MEK5 PB1 tightly with a K_d of about 10^{-8} M. Mutagenesis analysis revealed that residues in the basic cluster of MEKK3 PB1 contributes differently to the PB1−PB1 interaction. Residues Lys 7 and Arg 5 play important roles in the interaction with MEK5 PB1. Taken together, this study provides new insights into structural details of MEKK3 PB1 and its binding properties with MEK5 PB1.

The highly conserved mitogen-activated protein kinases (MAPKs) superfamily is one of the major systems participating in the transduction of signals from the cell membrane to nuclear and other intracellular targets (*1*). Some members of MAPKs family are involved in the pathogenesis of various processes, and many of them have been identified as attractive targets for therapeutic interventions in inflammatory, immunoresponsive diseases, and oncology (*1*−*4*). MEKK3,[1] also known as MAP3K3, is a member of the three-tiered kinase cascade. It is widely expressed and is an effective activator of the NF-κB pathway, in which it acts as an essential signal transducer of the MyD88−IRAK−TRAF6 complex in IL-1R−TLR4 signaling (*5*, *6*). MEKK3 also plays an essential role in the activation of ERK5 signal pathway by phosphorylating and activating its downstream MAPK kinase, MEK5, which in turn phosphorylates and activates the downstream MAPK ERK5 in the signaling cascade (*7*, *8*).

Both MEKK3 and MEK5 possess a PB1 domain in the N terminus. The PB1 domain is a modular domain mediating protein−protein interaction in a variety of biological events, typically via homo- or heterodimerization (*9*−*16*). Moreover, it is also involved in the interaction with other proteins (*17*, *18*). PB1 domains are classified into two types, I and II. Type I PB1 domains, such as MEK5 PB1, have a negatively charged acidic cluster, the OPCA motif, in the back end; while type II PB1 domains, including MEKK3 PB1, have a positively charged basic cluster in the front end. Type II PB1 domain binds type I PB1 domain to form a heterodimer in a front-to-back manner via electrostatic interaction (*16*). Some other PB1 domains containing both the OPCA motif and the basic cluster, such as aPKC and TFG, are classified as type I and type II. The PB1−PB1 interaction is highly specific and exclusive in spite of its electrostatic essence (*16*, *19*).

MEKK2, another member of the MAP3Ks, shares 76% sequence similarity with MEKK3. It also contains a type II PB1 domain in the N terminus. The PB1 domains of MEKK2 and MEKK3 are highly conserved, with 77% sequence similarity, and their binding modes to MEK5 PB1 are almost identical (*8*, *20*). The PB1-mediated ternary complex MEKK2 (MEKK3)−MEK5−ERK5 plays a key role in the stringent control of ERK5 activation, which is unique for ERK5 and not observed in the control of other MAPKs (*21*). In the ternary complex, MEKK2 (MEKK3) binds the C-terminal moiety of the MEK5 PB1, while ERK5 binds the N-terminal

[†] This work was supported by the Chinese National Fundamental Research Project (Grants 2002CB713806, 2006CB806507, and 2006CB910201) and the Chinese National Natural Science Foundation (Grants 30121001, 30570361, and 30670426).

[‡] Atomic coordinates have been deposited in the RCSB Protein Data Bank under accession codes 2PPH and 2JRH. NMR assignments have been deposited in the BioMagResBank under accession numbers 15355 and 15332.

* To whom correspondence should be addressed at the School of Life Sciences, University of Science and Technology of China, Hefei, Anhui 230026, People's Republic of China. Tel 86-551-3607464; fax 86-551-3601443; e-mail yyshi@ustc.edu.cn (Y.S.) or wujihui@ustc.edu.cn (J.W.).

[1] Abbreviations: MEKK3, MAP/Erk kinase kinase 3; MEK5, MAP/Erk kinase 5; ERK5, extracellular signal-regulated kinase 5; MAPK, mitogen-activated protein kinase; PB1 domain, Phox and Bem1p domain.

10.1021/bi701341n CCC: $37.00
Published on Web 11/07/2007

moiety and residues 117−131 C-terminal to the PB1 domain (*21*, *22*). Genetic inactivation of MEKK3, MEK5, ERK5, or the transcription factor MEF2C in mice unexceptionally gives rise to an embryonic lethal phenotype characterized by defects in angiogenesis and early cardiovascular development (*20*).

Although the crystal structures of free MEKK3 PB1 and its complex with MEK5 PB1 have both been deposited into the PDB data bank (PDB accession numbers 2C60 and 2O2V), there is no detailed report about their interaction. Here we have determined the solution structure of MEKK3 PB1 and revealed an interesting proline isomerization in the MEKK3 PB1 domain that is different from the crystal structures. We further studied backbone dynamics of MEKK3 PB1 and its binding properties with MEK5 PB1. A series of site-directed mutants targeted to different residues in the basic cluster was also designed, and their binding properties with MEK5 PB1 were studied by isothermal titration calorimetry (ITC). Our results demonstrated that these residues contribute quite differently to the domain interaction.

MATERIALS AND METHODS

Protein Expression and Purification. The human MEKK3 PB1 (42−126) and MEK5 PB1 (7−107) coding regions were obtained by PCR from a human HeLa cDNA library (Clontech) based on the mRNA sequences of human MEKK3 and MEK5, respectively. The primers for MEKK3 PB1 were 5′-CTAGCCATATGCAGAGTGACGTCAG-3′ and 5′-GTACTCGAGGT TTCTGTCCTGGGA-3′; and those for MEK5 PB1 were 5′-CTAATCATATGGGCCCCTTTCCTGC-3′ and 5′-G CGCTCGAGTCTTGGAAATATCTGC-3′, respectively. The amplified MEKK3 PB1 and MEK5 PB1 DNA fragments were inserted between *Nde*I/*Xho*I sites of pET22b (Novagen) and p28 (modified from pET28a, Novagen), respectively. The recombinant vectors of MEKK3 PB1 and MEK5 PB1 were then transformed into the *Escherichia coli* bacterial strain BL21 (DE3) and Rosetta, respectively.

Wild-type MEKK3 PB1 with a C-terminal His tag (LEHHHHHH) was expressed in *E. coli* BL21 (DE3) cells for large-scale protein production. His-tagged proteins were purified by a Hitrap chelating column (Pharmacia) according to the manufacturer's instructions. MEKK3 PB1 mutants and MEK5 PB1 were expressed in Rosetta cells.

MEKK3 PB1 Mutant Proteins. Site-directed MEKK3 PB1 mutants were made in pET22b(+) by oligonucleotide-based mutagenesis. DNA sequencing confirmed all PCR constructs, and the clones containing undesired mutations were discarded. The mutated proteins were all identified by matrix-assisted laser desorption ionization time-of-flight (MALDI-TOF) mass spectroscopy. ^{15}N-Heteronuclear single quantum coherence (HSQC) spectra indicated structural stability was maintained in the mutant proteins.

NMR Sample Preparation. Uniformly labeled recombinant MEKK3 PB1 was overproduced in 1000 mL of medium containing 0.5 g/L 99% ^{15}N-ammonium chloride and 2.5 g/L 99% ^{13}C-glucose as the sole nitrogen and carbon sources, respectively. The labeled proteins were also purified with Ni-chelating column.

Purity Identification and Concentration Measurement. The purities of all proteins were confirmed by SDS−PAGE and the concentrations were measured with BCA kits (Pierce). The ^{15}N-labeled and ^{13}C, ^{15}N-labeled MEKK3 PB1 were about 0.5 mM. The samples for NMR were buffered in 50 mM sodium phosphate (pH 6.0), 50 mM NaCl, and 1 mM ethylenediaminetetraacetic acid (EDTA) in 90% H_2O, 10% D_2O.

NMR Spectroscopy and Structure Calculations. The following spectra were recorded to obtain backbone and side-chain resonance assignments: 2D ^{1}H,^{15}N-HSQC, 3D ^{15}N-edited Nuclear Overhauser effect spectroscopy (NOESY)−HSQC (110 ms mixing time), 3D HNCO, 3D HN(CA)CO, 3D CBCA(CO)NH, 3D CBCANH, 3D H(C)(CO)NH−total correlation spectroscopy (TOCSY), 3D (H)C(CO)NH−TOCSY, and 3D HBHA(CBCACO)NH. All NMR experiments were recorded at 298 K on a Bruker DMX 600 spectrometer equipped with cryoprobe.

The ^{15}N-labeled sample was lyophilized and dissolved in 99.96% D_2O, followed immediately with HSQC experiments to monitor the disappearance of NH signals at 298 K. After all of the peaks vanished, 3D HCCH−TOCSY, 3D HCCH−COSY, and 3D ^{13}C-edited NOESY−HSQC (110 ms mixing time) were recorded on the same sample at 298 K. NMR data processing was carried out with NMRPipe and NMRDraw software, and the data were analyzed with SPARKY.

NMR distance restraints were collected from two different NOESY spectra: 3D ^{15}N-separated NOESY in water for amide protons, and 3D ^{13}C-separated NOESY in D_2O for aliphatic protons. The TALOS (torsion angle likelihood obtained from shift and sequence similarity) (*23*) was calculated for five types of nuclei: $^{13}C_\alpha$, $^{13}C_\beta$, ^{13}CO, $^1H_\alpha$, and ^{15}N. Only TALOS "good" predictions with nine or 10 matches in agreement were used and converted into restraints on ψ and φ angles. The chemical shift index (CSI) (*24*), which was calculated for four types of nuclei, $^{13}C_\alpha$, $^{13}C_\beta$, ^{13}CO, and $^1H_\alpha$, was applied as supplement. Hydrogen-bond restraints were obtained by identifying the slow-exchange amide protons after overnight incubation following solvent exchange. For each hydrogen bond, two distance restraints (NH−O and N−O) were used. Structures were calculated by the program CNS v1.1, employing a simulated annealing protocol for torsion angle dynamics. The calculated structures were analyzed by the programs PROCHECK and MOLMOL (*25*, *26*).

Chemical Shift Perturbation. For the chemical shift perturbation experiments, 0.2 mM ^{15}N-labeled wild-type MEKK3 PB1 was titrated with 46 mg/mL unlabeled MEK5 PB1. The ^{1}H and ^{15}N resonance variations were followed by HSQC experiments, and the NMR ^{15}N-HSQC spectra were acquired at 303 K.

NMR Backbone Relaxation Experiments. ^{15}N relaxation experiments were carried out at 303 K on a Bruker DMX500 NMR spectrometer. ^{15}N relaxation measurements were carried out by published methods (*27*). ^{15}N T_1 relaxation rates were measured with seven relaxation delays: 11.5, 61.3, 141.5, 362.2, 522.7, 753.4, and 1144.5 ms. ^{15}N T_2 relaxation rates were measured with six relaxation delays: 17.6, 35.2, 52.8, 70.4, 105.6, and 140.8 ms. The spectra measuring ^{1}H−^{15}N NOE were acquired with a 2-s relaxation delay followed by a 3-s period of proton saturation. The spectra recorded in the absence of proton saturation employed a relaxation delay of 5 s. The exponential curve fitting and extracts of

T_1 and T_2 were processed by Sparky. The relaxation data R_1/T_1, R_2/T_2, and NOE were analyzed by Fast ModelFree v4.15 (*28*).

Surface Plasmon Resonance. For the SPR analysis (*29*), association and dissociation of the MEKK3 PB1 domain with the MEK5 PB1 domain were measured with a BIAcore 3000 instrument (BIAcore AB, Uppsala, Sweden). MEK5 PB1 was coupled to a carboxymethyl-dextran CM5 sensor chip with an amine coupling kit (BIAcore AB, Uppsala, Sweden) containing 1-ethyl-3-[(3-dimethylamino)propyl]carbodiimide (EDC), *N*-hydroxysuccinimide (NHS), and ethanolamine. After the chip was activated by 35 μL of EDC/NHS mixture, MEK5 PB1 was coupled to the CM5 sensor surface with about 35 μL of protein (1 μM) in the immobilization buffer (10 mM acetate, pH 5.0). The binding assay was performed at a constant flow rate of 30 μL/min at 298 K with MEKK3 PB1 concentrations in the range of 0−3.63 μM. The running buffer is 50 mM PO_4^{3-} and 100 mM NaCl (pH6.0). NaOH (5 mM) was used to regenerate the chip. For fitting of the binding kinetics, BIAevaluation version 4.1 software (BIAcore AB) was applied, and the 1:1 Langmuir binding model was chosen.

Isothermal Titration Calorimetry. ITC measurements (*30*, *31*) were carried out at 303 K on a VP−ITC titration calorimeter (MicroCal, Northampton, MA). All solutions were thoroughly degassed before use by stirring under vacuum. The sample cell was loaded with 1.43 mL of MEK5 PB1 (0.012−0.015 mM, in 50 mM PO_4^{3-} and 100 mM NaCl, pH 7.0), and the reference cell contained doubly distilled water. Titration was carried out by use of a 279-μL syringe filled with wild-type or mutant MEKK3 PB1 solution (50 mM PO_4^{3-} and 100 mM NaCl, pH 7.0). The concentrations of MEKK3 PB1 or the mutant proteins were varied between 0.3 and 0.5 mM. To correct for the heat effects not directly related to the binding reaction (dilution, change in the degree of protonation of the ligand, etc.), control experiments were performed by making identical injections of MEKK3 PB1 or mutant protein solution into the titration cell containing only buffer. The heat due to the binding reaction between the two proteins was obtained as the difference between the heat of reaction and the corresponding heat of dilution. At pH 7.0, the experiments were carried out in the same way. The obtained heat signals from the ITC were integrated by use of Origin software supplied by MicroCal Inc. Reversed assays were performed for all samples.

RESULTS AND DISCUSSION

Solution NMR Spectroscopy Revealed a Proline Cis−trans Isomerization of MEKK3 PB1. The ^{1}H-^{15}N HSQC spectrum of MEKK3 PB1 was well-dispersed, indicating a well-folded protein domain. Unexpectedly, the spectra exhibited a set of cross-peaks with relatively low intensity in addition to the major ones (Figure 1A). The population of the minor peaks was about 12% according to the signal intensity ratio. Sequence assignment of the spectra by triple resonance experiments revealed that almost a third of the amide signals were duplicated. A monomer/dimer equilibrium should be excluded as a source of the extra signals according to gel-filtration chromatography (Supporting Information) and ^{15}N amide T_2 relaxation measurement (Figure 4B), both of which indicated that MEKK3 PB1 was a homogeneous monomer in solution under the conditions used for structural determination by NMR. Therefore, an intramolecular conformation exchange was the only possible reason for the low-intensity signals in the spectra.

As an important clue, the chemical shift differences for backbone amides between the minor and the major conformations became larger as the residues got closer to residue Pro39 (Figure 1B). Because cis/trans isomerization of the prolyl peptide bond is a relatively slow process due to the partial double bond character of the C−N bond, it may result in two separate signals for each residue affected by the isomerization in NMR spectra. Taking these into consideration, we speculated that cis/trans isomerization around the Gln38−Pro39 imide bond may be the source of the conformational heterogeneity. Consistent with this hypothesis, characteristic NOEs for both cis and trans conformations of the Gln38−Pro39 bond were observed in the ^{13}C-edited NOESY spectrum (Figure 1C). Furthermore, the chemical shift differences between $^{13}C_\beta$ and $^{13}C_\gamma$ nuclei were 8.4 ppm for the cis conformation and 3.7 ppm for the trans conformation of Pro39 (Figure 1D), which were in agreement with the average values (9.64 ± 1.27 ppm for *cis*-Xaa−Pro and 4.51 ± 1.17 ppm for *trans*-Xaa−Pro) estimated from statistical analysis of ^{13}C chemical shifts of proline in proteins (*32*).

NMR Structure Determination of MEKK3 PB1 Domain. The solution structure of the recombinant protein MEKK3 PB1 domain was determined by multidimensional heteronuclear NMR spectroscopy. The relatively low population of the cis isomer increased the difficulty of both spectral assignment and structure calculation. However, we were able to assign an efficient number of characteristic NOEs corresponding to secondary structures, as well as a number of medium- and long-range NOEs. The calibration of distance constraints for the cis isomer was achieved on the basis of characteristic distances in the secondary structures. Figure 2A shows an ensemble of 20 lowest energy NMR structures for both isomers.

Table 1 lists the structure statistics for a family of 20 structures for both isomers. For residues 4−68 and 75−80, the root-mean-square deviation (rmsd) from the mean structure are 0.547 Å (trans) and 0.622 Å (cis) for the backbone C_α, C′, and N atoms. Residues 69−74 in the loop region are flexible, and few restraints were obtained in this region. Resonances of K70 and K73 are very weak in the 2D ^{1}H−^{15}N HSQC, possibly owing to fast exchange of their amide hydrogens with the solvent. A PROCHECK (*26*) analysis of the 20 NMR structures indicated that >98% (trans) and >97% (cis) of the residues lie in the most favored region and additional allowed region of the Ramachandran plot. Residues in the disallowed regions are those at the termini or in the loops because of the sparsity of interresidual NOEs.

Structure Description of MEKK3 PB1 Domain. Each isomer of MEKK3 PB1 folds into a compact globular domain of five β-strands and two α-helices. The five β-strands are arranged in a twisted parallel and antiparallel β-sheet constituted of residues Val4−His10 (β1), Glu13−Phe19 (β2), Asp41−Met45 (β3), Ser50−Leu52 (β4), and Leu75−Leu80 (β5). The two α-helices, α1 (Tyr25−Phe36) and α2 (Gln56−Arg68), are nearly orthogonal to each other and lie at the opposite side of the β-sheet (Figure 2B). The structure is

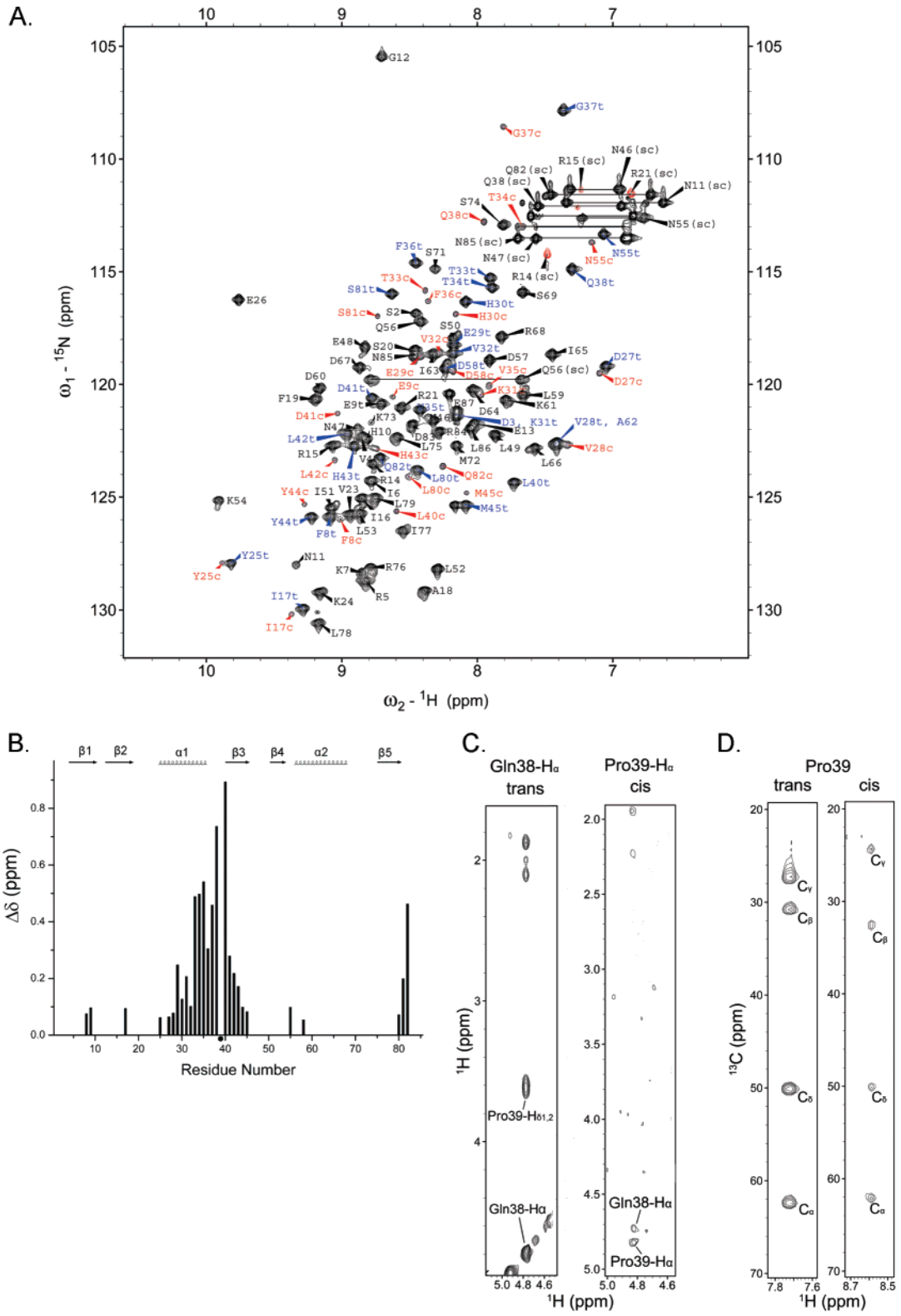

FIGURE 1: Proline isomerization of MEKK3 PB1 domain. (A) Two-dimensional ^{1}H−^{15}N HSQC spectrum of the wild-type MEKK3 PB1 at 50 mM NaCl, 50 mM sodium phosphate buffer, pH 6.0, and 25 °C. Assignments are included for all the backbone NH pairs. Resonances corresponding to cis and trans conformations are labeled as c (red) and t (blue), respectively; resonances without isomerization are labeled in black. The population of the minor peaks is about 12% (average signal/noise ratios for the minor and major peaks are about 28 and 190, respectively). Side-chain NH resonances of Arg and side-chain NH_2 resonances of Asn and Gln are labeled as (sc). Side-chain NH resonances of Arg are folded cross-peaks in the spectrum and are shown in red. (B) Chemical shift difference ($\Delta\delta$) between the cis and trans isomers of MEKK3 PB1, plotted as a bar graph. $\Delta\delta$ was calculated using the formula $\Delta\delta = [(0.17\Delta\delta_N)^2 + \Delta\delta_H^2]^{1/2}$, where $\Delta\delta_N$ and $\Delta\delta_H$ denote the chemical shift differences of nitrogen and hydrogen between the two isomers, respectively. (•) indicates residue Pro39. (C) Characteristic NOE cross-peaks from ^{13}C-edited NOESY spectra between the Gln38-H$_\alpha$ and Pro39-H$_{\delta1,2}$ protons for the trans conformation and between Gln38-H$_\alpha$ and Pro39-H$_\alpha$ protons for the cis conformation. The much lower signal intensity of cis isomer is due to much lower population. (D) Strips from the CCO−NH spectra showing the ^{13}C chemical shifts of Pro39 carbon backbone. The chemical shift difference between $^{13}C_\beta$ and $^{13}C_\gamma$ nuclei for the cis and trans conformations of residue Pro39 of MEKK3 PB1 are 8.4 and 3.7 ppm, respectively.

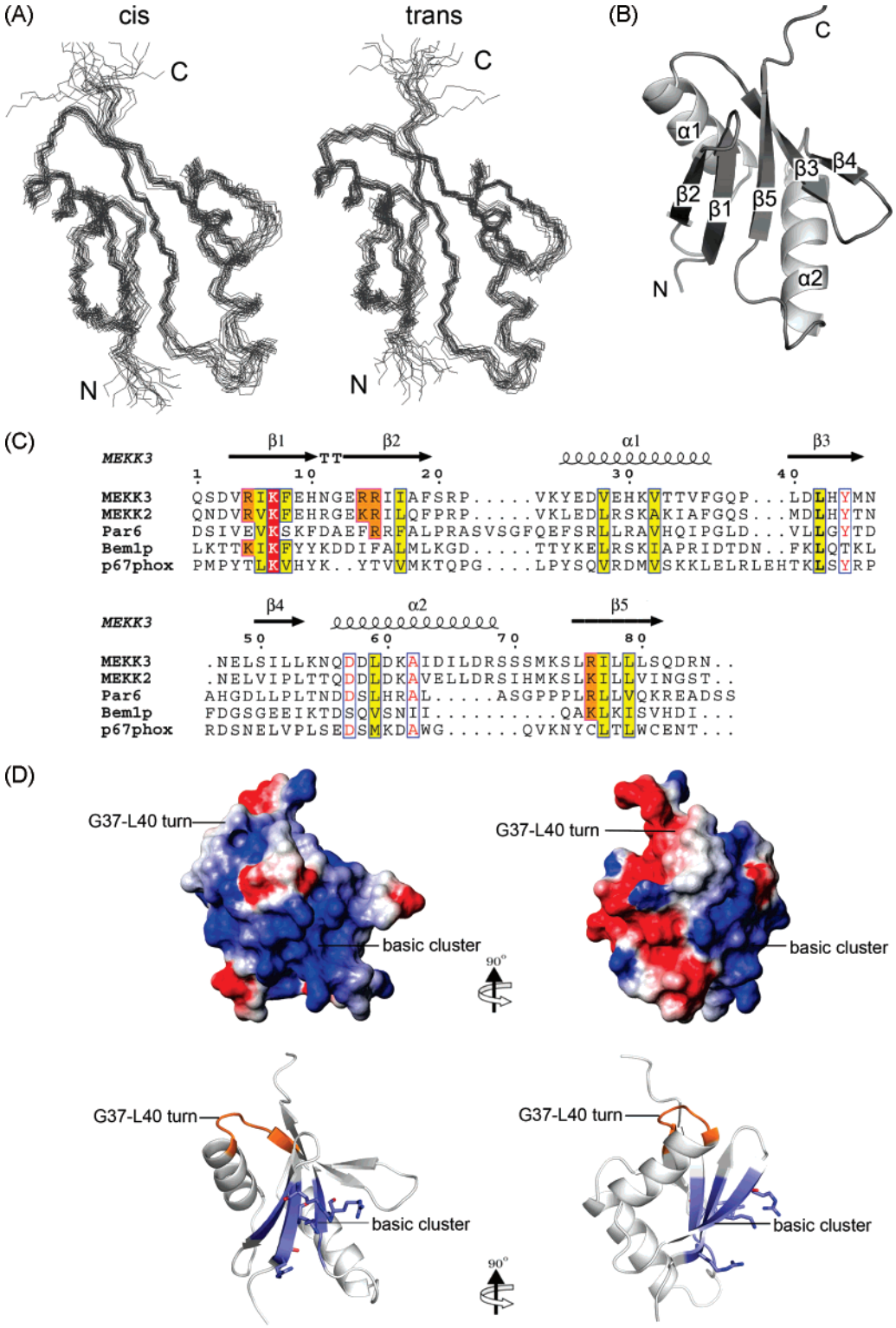

FIGURE 2: Solution structure of MEKK3 PB1 domain. (A) Backbone superposition of 20 selected cis (left) and trans (right) isomers from the final CNS calculation of the NMR structure. N and C termini are indicated as N and C, respectively. These figures were generated with MOLMOL (*25*). (B) Cartoon representation of the energy-minimized average structure of the trans conformation, with secondary structure elements highlighted. The cis conformation has the same secondary structural arrangement as the trans conformation. This figure was generated with PyMOL. (C) Sequence alignment of MEKK3 PB1 with other representative type II PB1 domain proteins. Bem1p is from *S. cerevisiae*, while the others are from *Homo sapiens*. Conserved hydrophobic residues forming a hydrophobic core are shown in yellow. The highly conserved lysine critical to the binding of type I PB1 domain is shown in red; basic residues participating in the interaction interface are shown in orange. The sequence alignment was made by use of ClustalW (*33*), and the figure was generated with ESPript 2.2 (*34*). (D) Electrostatic surface potential of the trans conformation (upper panel) and a cartoon representation with the isomerization region and the binding surface with MEK5 PB1 highlighted (lower panel). In the upper panel, blue in the front shows a positively charged cluster, while negatively charged and neutral residues are represented in red and white, respectively. In the lower panel, the binding interface with MEK5 PB1 is far away from the G37−L40 turn, where the proline isomerization occurs. The secondary structure arrangement and electrostatic surface potential of the cis isomer are the same as those of the trans isomer. These figures were generated by use of software MOLMOL (*25*) and PyMOL (http://www.pymol.org), respectively.

Table 1: Structural Statistics of MEKK3 PB1 Cis and Trans Isomers

	trans	cis
NMR Restraints		
distance restraints	1225	1184
intraresidue ($i-j=0$)	385	382
sequential ($\|i-j\|=1$)	332	325
medium range ($2 \le \|i-j\| \le 4$)	209	203
long range ($\|i-j\| \ge 5$)	271	246
hydrogen bonds	28	28
dihedral angle restraints	110	112
Mean rms Deviations from Idealized Covalent Geometry		
bond (Å)	0.0007 ± 0.000 03	0.0008 ± 0.000 03
angle (deg)	0.2816 ± 0.0007	0.2883 ± 0.0011
improper (deg)	0.0895 ± 0.0017	0.0950 ± 0.0031
Lennard-Jones potential energy (kcal mol^{-1})	−296.05 ± 12.70	−273.7 ± 12.49
Distribution of Residues in Ramachandran Plot[a] (%)		
most favorable regions	87.8	88.3
additional allowed regions	10.3	9.5
generously allowed regions	1.4	1.6
disallowed regions	0.5	0.6
Atomic rms Differences[b] (Å) (Residues 4−68 and 7−80)		
backbone heavy atom (N, C$^{\alpha}$, and C′)	0.547	0.622
heavy atoms	1.35	1.43

[a] The program Procheck was used to assess the overall quality of the structures. [b] The precision of the atomic coordinates is defined as the average rms difference between the 20 final structures and the mean coordinates of the protein. [c] None of the structure exhibits distance violations greater than 0.5 Å or dihedral angle violations greater than 5°.

stabilized by a hydrophobic core consisting of a large number of residues including Ile6, Phe8, Ile17, Val28, Val32, Leu42, Leu59, Ile77, and Leu79, all of which are highly conserved throughout type II PB1 domains (Figure 2C). Analysis of the electrostatic surface potential showed that the interaction interface for MEK5 PB1 on β1 and β2 is highly positively charged (Figure 2D).

The major backbone differences between the cis and trans conformations lie in the G37−L40 turn connecting α1 and β3, the region where Pro-39 is located (Figure 2D). In the cis form, it adopts a type VIb β-turn, according to the criteria that the distance between the $C_{\alpha(i)}$ and $C_{\alpha(i+3)}$ is less than 7 Å and the residues are not helical, together with ψ and φ angle characters (*35*); in the trans conformation, this region does not belong to any typical type of β-turn as the distance from $C_{\alpha G37}$ to $C_{\alpha L40}$ has exceeded 7 Å (Figure 3A). The side chain of Gln38 is pointing in opposite directions in the two isomers; it is close to residue Thr33 in the cis isomer but far from it in the trans isomer (Figure 3B). As a result, a characteristic NOE for $H_{\alpha P39}-H_{\alpha T33}$ was observed in the trans conformation, while in the cis form, an unambiguous NOE correlation between $H_{\gamma T33}$ and $H_{\beta Q38}$ was present in the ^{13}C-edited NOESY spectrum (Figure 3C).

Although the principal structure difference between cis and trans conformations is confined to the β-turn region, the chemical shift differences extend to a much larger range, possibly because of a shift of the electron distribution resulting from partial rearrangement of the side chains close to Pro39.

Backbone Dynamics of MEKK3 PB1 from ^{15}N Relaxation Measurements. The backbone dynamics of MEKK3 PB1 from ^{15}N relaxation experiments is consistent with the results of structure calculation. The ^{15}N relaxation data for the trans

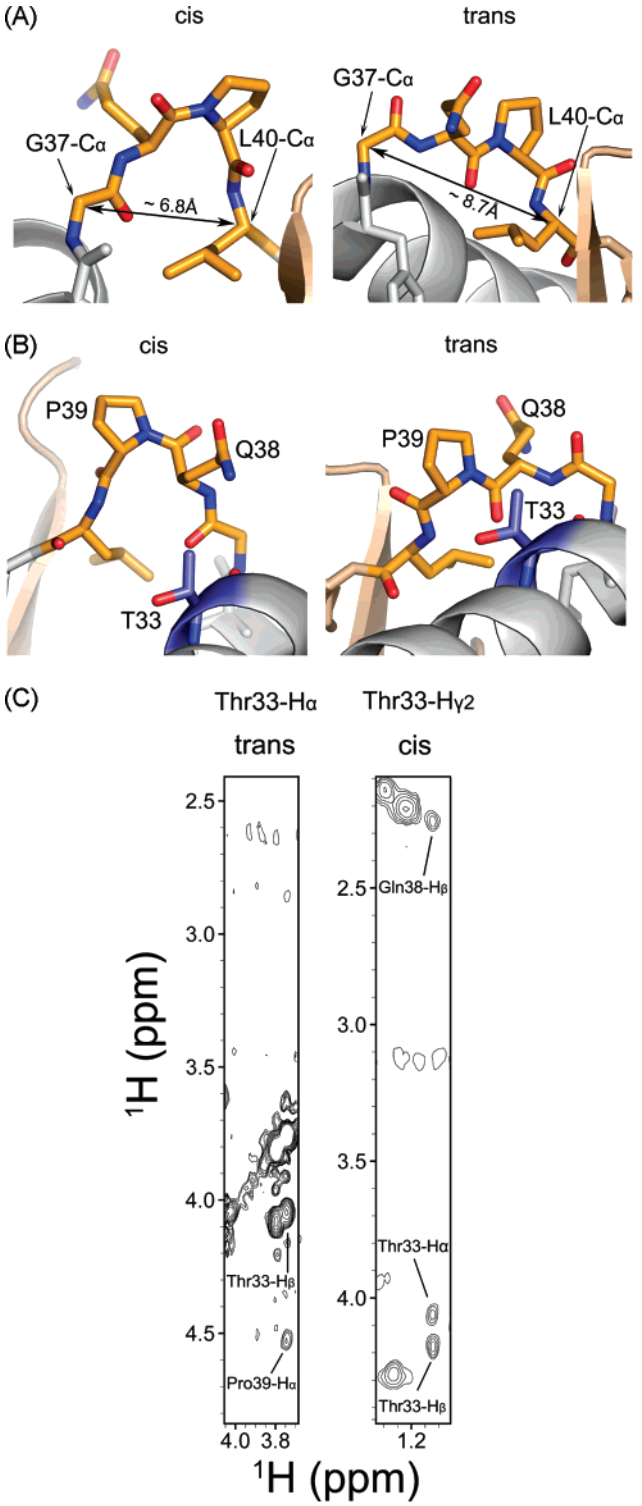

FIGURE 3: Major difference between cis and trans isomers of MEKK3 PB1 domain. (A) Residues G37−L40 in the cis conformation (left) form a type VIb β-turn, which in most cases requires a Pro for stabilization. The distances between $C_{\alpha G37}$ and $C_{\alpha L40}$ in the cis (left) and trans (right) conformations are about 6.8 and 8.7 Å, respectively. (B) Different arrangements of the Gln38−Pro39 bond in cis and trans conformations. In the trans form (right), the side chain of Gln38 is away from Thr33, whereas in the cis form (left), Gln38 points to and approaches Thr33. These figures were generated with PyMOL. (C) NOE cross-peaks from ^{13}C-edited NOESY spectra between Thr33-H_{α} and Pro39-H_{α} proton for the trans conformation and between Thr33-$H_{\gamma 2}$ and Gln38-$H_{\beta 1,2}$ for the cis conformation further corroborate that the structural heterogeneity of MEKK3 PB1 is caused by the isomerization of the Gln38−Pro39 bond.

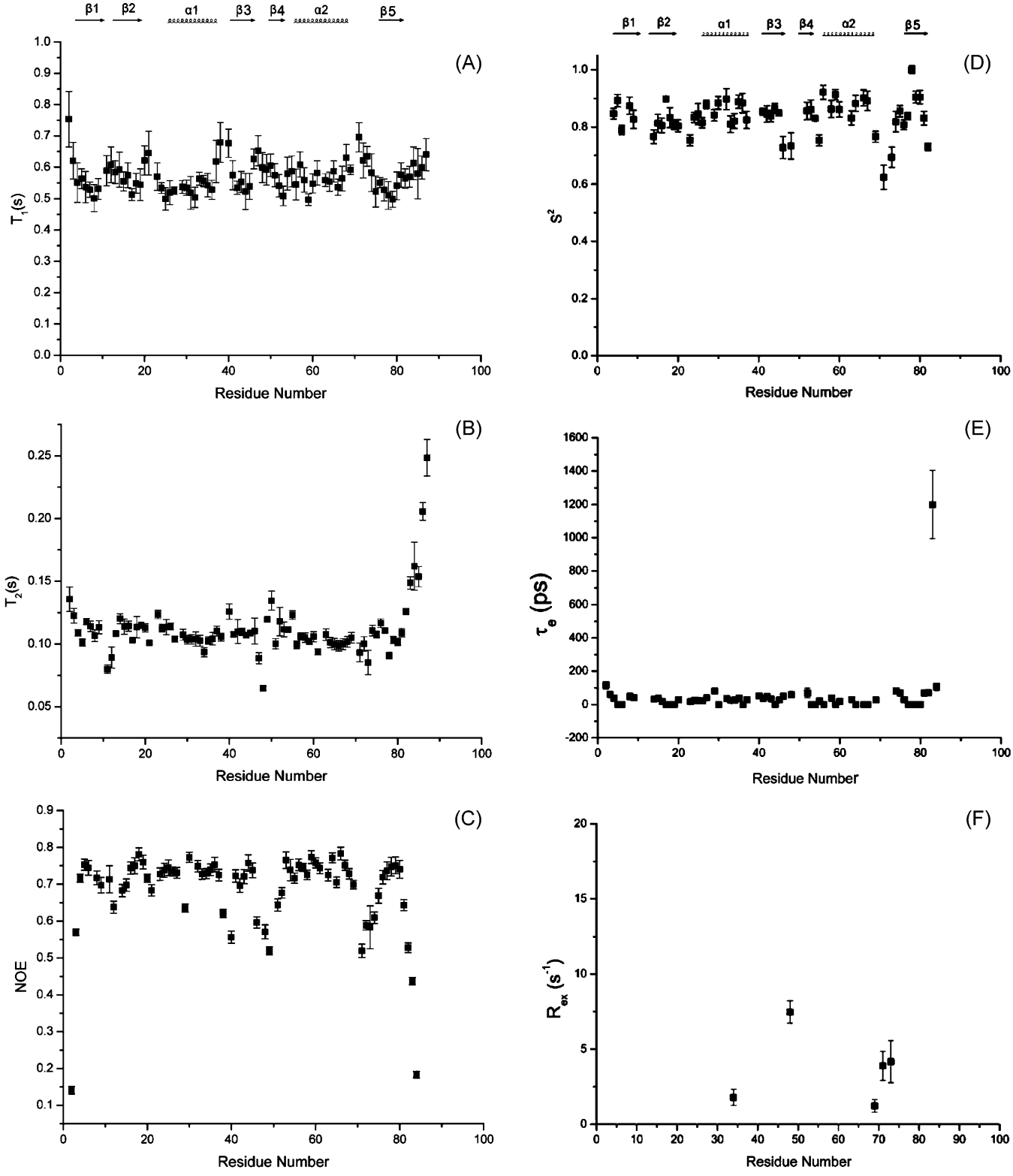

FIGURE 4: Backbone dynamics of MEKK3 PB1. (A−C) Backbone ^{15}N relaxation data T_1, T_2, and steady-state $\{^1H\}-^{15}N$ NOEs for the trans conformation at 500 MHz are plotted against residue number. Standard deviations are presented as error bars. Secondary structure of MEKK3 PB1 is demonstrated at the top. (D−F) S^2, τ_e, and R_{ex} analyzed by FAST ModelFree. Data are plotted versus residue number. Secondary structure of MEKK3 PB1 is indicated at the top.

isomer are shown in Figure 4A−C. However, we failed to obtain reliable relaxation data for the cis isomer because of the much lower intensities of minor cross-peaks. T_1 and T_2 relaxation times along with steady-state $\{^1H\}-^{15}N$ NOE were determined for 72 out of 83 non-proline residues and plotted as a function of the sequence. Of the 11 undetermined residues, Gln1, Ser70 were too weak to obtain reliable data and the other nine residues were overlapped in the spectra.

Generalized order parameters S^2 were obtained for 61 residues by Fast ModelFree v4.15; the other residues were unfit for Fast ModelFree software (Figure 4D). The generalized order parameter S^2 is a measure of the amplitude of fast internal motion in a macromolecule, while the effective

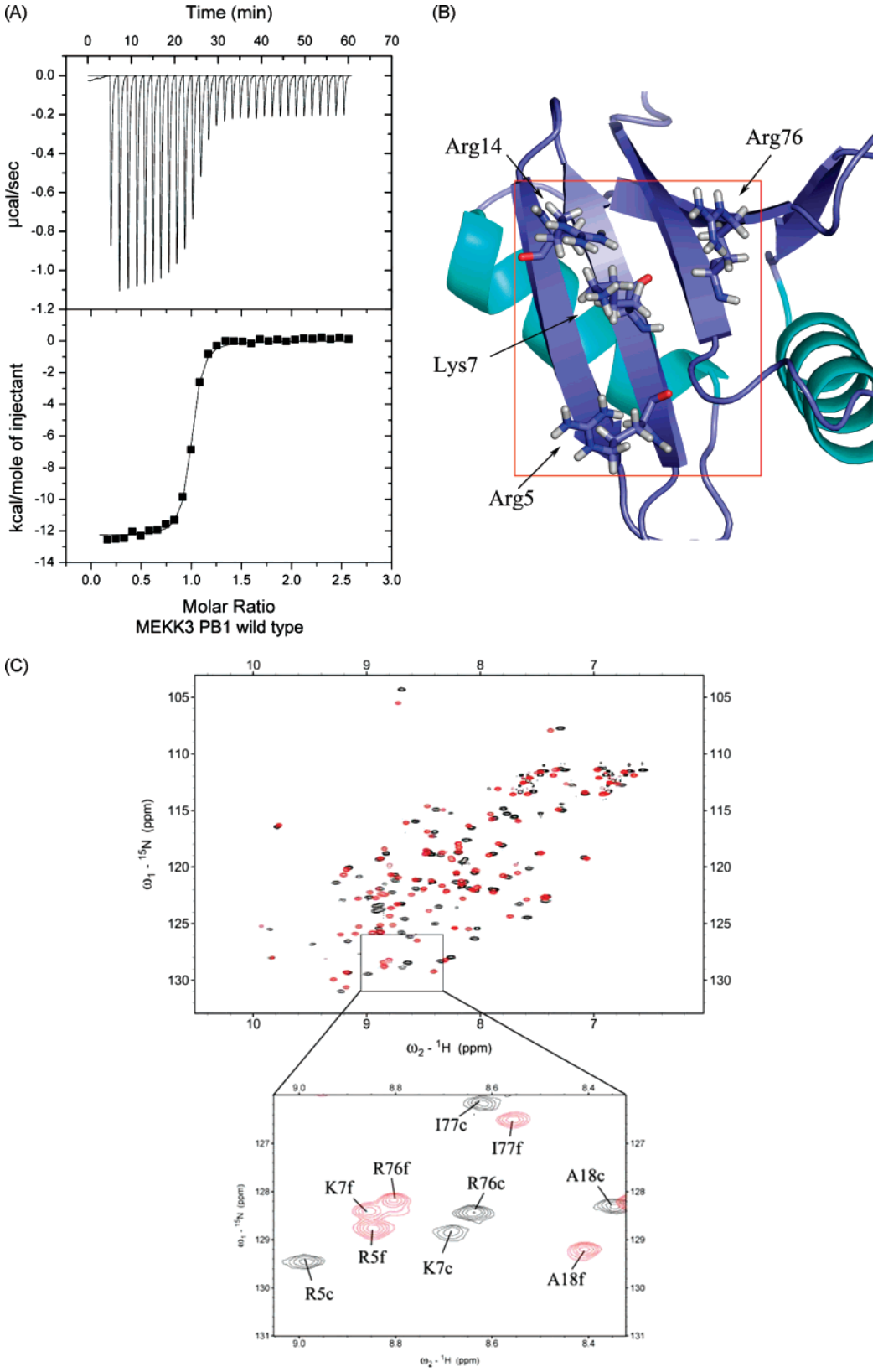

FIGURE 5: Strong binding of MEKK3 PB1 to MEK5 PB1. (A) Thermodynamic analysis of MEKK3 PB1/MEK5 PB1 interaction by ITC. The top panel shows heat release during titration of aliquots of MEKK3 PB1 into MEK5 PB1 at 303 K, pH 7.0, corrected for baseline drift. The bottom panel shows the integrated heat of binding. Data were fitted to a single binding site model after the heat of dilution was subtracted. Concentrations of MEKK3 PB1 and MEK5 PB1 were 0.3587 and 0.015 mM, respectively. (B) Interaction interface of MEKK3 PB1. Residues R5, K7, R14, and R76 in the red box constitute the positive charge cluster of MEKK3 PB1. This figure was generated with PyMOL. (C) Overlay of 2D $^{1}H-^{15}N$ HSQC spectra of MEKK3 PB1 in free state (labeled f, in red) and the complex with unlabeled MEK5 PB1 (labeled c, in black). Molar ratio of ^{15}N-labeled MEKK3 PB1 to unlabeled MEK5 PB1 was 1:1. Resonances of residues R5, K7, and R76 in the interaction interface underwent obvious changes upon binding of MEK5 PB1. To highlight the difference between free and complexed states, a higher level of contours was adopted in the $^{15}N-^{1}H$ HSQC spectra; thereby only the resonances for the trans isomer of MEKK3 PB1 are visible.

correlation time τ_e (Figure 4E) is a measure of the rate of motion (*36*). The average S^2 value was 0.84(±0.02), indicating that most regions of MEKK3 PB1 are relatively rigid. Residues participating in regular secondary structures are characterized by high S^2 (>0.75) and low τ_e values (<50 ps), which reflects fast librational motions. Residues in the termini and loops, especially the α2/β5-loop (residues 69−74), exhibited reduced $^1H-^{15}N$ NOE values and order parameters ($S^2 < 0.7$), and an extra average R_{ex} of 3.1 s^{-1} (Figure 4F), indicating distinct microsecond−millisecond internal motions in their environment. Accordantly, the conformation for this region was poorly defined in the calculated ensemble. In addition, the β3/β4-turn (residues 46−49) of MEKK3 PB1, which is close to the counterpart region of the acidic cluster of MEK5 PB1, also exhibited lower $^1H-^{15}N$ NOE values, reduced order parameters (S^2), obviously reduced T_2 (less than 100 ms), and interestingly high R_{ex} (7.4 s^{-1}). These together characterized evident internal motions on microsecond−millisecond time scale in this region. Further, the Pro39 region showed no obvious extra internal motions due to the inherent slow process of proline isomerization which is typically on a second−minute time scale (*37*, *38*).

A Stable Complex Formed between Wild-Type MEKK3 PB1 and MEK5 PB1. Due to the essential role of PB1−PB1 interaction in the activation of ERK5 signaling pathway (*8*), we attempted to study their binding properties. The results of both GST pull-down assay and gel-filtration chromatography indicated that MEKK3 PB1 strongly binds to MEK5 PB1 and may form a stable complex (Figures SI-1 and SI-2, Supporting Information). These results provoked us into more detailed investigation of their binding characteristics.

The binding thermodynamics of MEKK3 PB1 to MEK5 PB1 was analyzed by surface plasmon resonance (SPR) and isothermal titration calorimetry (ITC) (Figure 5A). The disassociation constant measured by ITC and SPR are 4.15×10^{-8} M and 1.29×10^{-8} M, respectively, implying a quite strong interaction. The measured disassociation rate constant (k_{off}) is 1.33×10^{-3} s^{-1}, and the association rate constant (k_{on}) is 1.05×10^5 M^{-1} s^{-1}. The slow k_{off} is consistent with the slow exchange in NMR titration (see following section). The binding free energy, which can be calculated from K_d, is composed of enthalpic (ΔH) and entropic ($-T\Delta S$) components ($\Delta G = \Delta H - T\Delta S$). These two terms can be obtained by nonlinear curve data fitting using Origin software supplied with the instrument. For the binding reaction occurring at 303 K in our experiments, ΔH was determined to be −12.30 kcal mol^{-1} (Table 2), while the corresponding entropic component ($-T\Delta S$) was 2.05 kcal mol^{-1}. Thus, the Gibbs free energy change of the binding process was calculated to be −43.05 kJ mol^{-1}. According to the second law of thermodynamics, this indicated that a stable complex should be formed between them.

Thermodynamic analysis from ITC experiments showed that the binding process is accompanied by highly favorable ΔH and slightly unfavorable ΔS. Moreover, the MEKK3 PB1 mutant R5A, which shows a dramatically reduced binding affinity to MEK5 PB1, also exhibits an obvious decrease in ΔH upon binding MEK5 PB1 in the ITC experiments (Figure 6). Thus, we propose that MEKK3 PB1 binding to MEK5 PB1 is enthalpically driven. Such favorable enthalpy changes of binding may arise from a large area of electrostatic interaction at the interface, while the unfavorable entropy changes presumably results from conformation restrictions of residues at the interface upon binding. Despite their strong interaction, we failed to solve the solution structure of the complex, probably because of aggregation of the complex at relatively high concentration for NMR experiments, which was also indicated by its relaxation data acquired at different concentrations (data not shown).

Table 2: Statistics of Thermodynamic Parameters from ITC Experiments on MEKK3 PB1 Mutants and MEK5 PB1[a]

mutation[b]	N[c]	K_d ($\times 10^{-8}$ M)	ΔH (kcal mol^{-1})	$-T\Delta S$ (kcal mol^{-1})
wild type	0.965 ± 0.003	4.15 ± 0.46	−12.31 ± 0.07	2.05
K7R	0.888 ± 0.006	37.0 ± 2.77	−13.61 ± 0.14	4.62
R5A	0.878 ± 0.010	164.7 ± 9.88	−7.37 ± 0.12	−0.64
R14A	0.891 ± 0.022	49.7 ± 11.4	−10.38 ± 0.34	1.61
R76A	0.863 ± 0.005	21.6 ± 1.92	−12.86 ± 0.12	3.55

[a] The ITC experiments were performed such that MEK5 PB1 was titrated with mutants and wild-type MEKK3 PB1. The results of the reversed assays are similar to these. [b] All five mutants and wild-type MEKK3 PB1 were included in the experiments. However, K7A mutant did not provide satisfactory results because the interaction is too weak. [c] Binding stoichiometry.

Different Significance of the Residues in the Basic Cluster of Interface Revealed by Analysis of Varied Mutants. It has been reported that the basic cluster in β1, β2, and β5 of type II PB1 domain is of great significance in heterodimer formation (*16*, *39*). On the basis of sequence alignment and structure comparison, we presumed that four primary residues including the highly conserved lysine were involved in the formation of MEKK3 PB1−MEK5 PB1 complex (Figure 5B). This was supported by the result of an NMR titration experiment in which residues in the interface underwent remarkable changes upon complex formation (Figure 5C). When the ^{15}N-labeled MEKK3 PB1 was titrated with unlabeled MEK5 PB1, most peaks experienced changes, in which a set of resonances disappeared while another set of peaks appeared, indicating a slow exchange on the NMR time scale.

To identify whether these residues contribute equally to the high binding affinity, a set of site-directed mutants, R5A, K7R, K7A, R14A, and R76A, were designed. Their binding affinities with MEK5 PB1 were measured by isothermal titration calorimetry. Consistent with previous studies (*8*, *20*), the K7A mutant considerably weakened the affinity with MEK5 PB1, while the K7R mutant sustained the strong binding affinity ($K_d = 3.7 \times 10^{-7}$ M) (Table 2). Binding affinity of the R5A mutant decreased greatly to 1.6×10^{-6} M (Table 2), suggesting an important role of R5 in the binding in spite of its lower conservation. In contrast, residues R14 and R76 appear to be of less significance in complex formation, even though they appear to be more conserved. Both R14A and R76A mutants bind to MEK5 PB1 with similar binding affinities ($K_d = 5.0 \times 10^{-7}$ M and 2.2×10^{-7} M, respectively), comparable to that of wild-type MEKK3 PB1.

The mutagenesis analysis is in accordance with the crystal structure of the heterodimer of MEKK3 PB1 and MEK5 PB1 (PDB accession number 2O2V). The crystal structure demonstrates that residue Lys7 of MEKK3 PB1 is located in the center of the binding interface and forms salt bridges with three Asp residues, and Arg 5 forms a salt

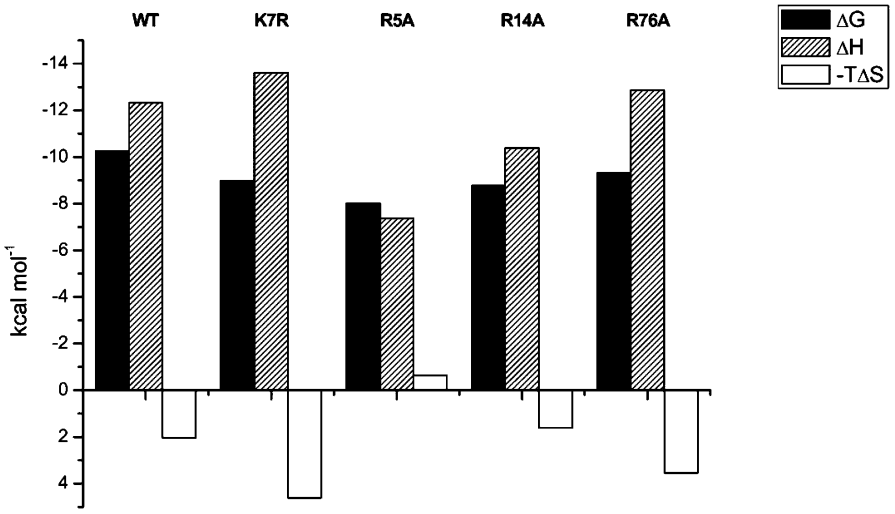

FIGURE 6: Comparison of thermodynamics between MEKK3 PB1 and its mutants in the interactions with MEK5 PB1. Thermodynamic parameters from ITC of wild-type MEKK3 PB1 and its mutants titrated into MEK5 PB1 are shown as bar plots. The obvious difference in ΔH between wild-type MEKK3 PB1 and R5A mutant is in accordance with their distinct binding affinities to MEK5 PB1. For illustration clarity, no error bars are shown.

bridge with a Glu residue in the OPCA motif of MEK5 PB1; these electrostatic interactions are all within 3 Å, whereas Arg 14 and Arg 76 lie on the edge of the interface and form weaker electrostatic interactions with MEK5 PB1. Our mutagenesis analysis proved that the positive charge of Lys7 is essential for the heterodimerization, and Arg 5 also plays an important role, whereas Arg14 and Arg76 contribute less to the binding. These results are in agreement with the crystal structure of the complex.

Interestingly, we have noticed a dramatic difference in the total heat of dilution of the mutants. Dilutions of R5A, K7A, R14A, and R76A mutants were endothermal, whereas wild-type MEKK3 PB1 and K7R mutant were exothermal when diluted with the same buffer (Figure SI-3, Supporting Information). A plausible explanation is that the replacement of lysine or arginine with alanine resulted in a decrease in the area of charged surface, and consequently reduced hydrophilicity. Furthermore, in contrast to R14A and R76A, very little reaction heat was generated in the titrations of R5A and K7A mutants, even at the beginning of the reactions. These results are in accordance with the lower binding affinities of R5A and K7A mutants with MEK5 PB1 and support that the binding process is enthalpically driven.

Comparison of Solution and Crystal Structures of MEKK3 PB1. During the period of our work, the crystal structures of MEKK3 PB1 both in the free state (PDB accession number 2C60) and in complex with MEK5 PB1 (PDB accession number 2O2V) were deposited into the Protein Data Bank. Comparison displayed a major difference between our solution structure and the crystal structures. Pro-39 was observed to undergo equilibrium between cis and trans conformations in the solution structures, while only the trans conformation was observed in the crystal structures. Presumably, the low population of cis isomer may be responsible for the lack of proline isomerization in crystal state. The other proline, Pro22, adopts a cis conformation in both solution and crystal structures.

Overall, MEKK3 PB1 experienced no obvious structural change upon MEK5 PB1 binding. An rmsd of 1.2 Å for the backbones was demonstrated by structural comparisons between the trans isomer of the solution structure and the crystal structures in both free and complexed states. Hence, the trans isomer of MEKK3 PB1 and its crystal structures are very alike except for the differences presented in the β3/β4-turn (residues 46−49) and α2/β5-loop (residues 69−74) where internal motions occur.

Structural Distinctions of MEKK3 PB1 and Its Implication. Although a number of crystal and NMR structures of PB1 domain have been solved, the MEKK3 PB1 is the first one showing a proline isomerization within the PB1 domain family. In addition, the other proline in MEKK3 PB1, Pro22, adopts cis instead of trans conformation. As the percentage of cis proline (about 6.5%) is significantly lower than the trans form based on statistic analysis of Xaa−Pro peptides (*40*), the concurrence of the two cis prolines in MEKK3 PB1 seems quite rare. However, both the cis and trans forms of MEKK3 PB1 bind to MEK5 PB1 with similar affinities because the signal intensity ratios of cis to trans isomer are nearly identical in free and complex states (data not shown); a plausible explanation is that the binding interface for MEK5 PB1 is opposite to and far away from the proline isomerization region (Figure 2D). Therefore the effect of Gln38−Pro39 bond isomerization on complex formation is negligible.

Among various MAPKs pathways, the MEKK2 (MEKK3)−MEK5−ERK5 pathway is somewhat unique in that it is PB1 domain-dependent (*21*). PB1 domains of MEKK2 and MEKK3 specifically bind to the PB1 domain of MEK5, and these interactions play a crucial role in the MEKK2- or MEKK3-mediated activation of ERK5 (*41*). Our study here has provided the structural basis of the interaction between MEKK3 PB1 and MEK5 PB1 in detail.

PB1 domains from different proteins are structurally similar; all adopt a ubiquitin-like β-grasp fold. MEKK2 PB1 and MEKK3 PB1 are even more similar, with a sequence similarity of 77%, and an rmsd of 1.59 Å in structural comparison. Despite the high similarity between MEKK2 PB1 and MEKK3 PB1, functional divergence has been unraveled very recently (*22*). MEKK2 PB1 was shown to bind MKK7 via its back-end acidic cluster, whereas MEKK3

PB1 was not found to bind an MKK other than MEK5. Hence, it remains unclear what potential function the MEKK3 PB1 domain back-end acidic cluster may have.

A notable structural divergence between the two MEKK PB1 domains is present in that residue Pro39 in MEKK3 PB1 undergoes equilibrium between cis and trans conformations whereas the corresponding residue in MEKK2 PB1 is a serine instead of proline. Furthermore, we have examined the HSQC spectrum of MEKK2 PB1 (Figure SI-4, Supporting Information) and its solution structure (PDB accession number 2CU1), and no evidence of multiconformation in MEKK2 PB1 has been found. Whether this structural difference between MEKK2 PB1 and MEKK3 PB1 is responsible for their functional difference is still unclear.

Proline isomerization has been reported in many proteins as a molecular switch regulating specific pathways (*42*−*44*). For example, in an adaptor protein Crk, a proline on the linker tethering two SH3 domains interconverts between cis and trans conformations, corresponding to the inhibited and activated conformations of Crk. In the cis conformation, the linker−$SH3^C$ region interacts intramolecularly with the $SH3^N$ domain, thereby preventing $SH3^N$-mediated Crk association with its biological partners, such as Abl. In contrast, in the trans conformation Crk exists in an open, uninhibited conformation. Thereby this proline isomerization results in negative regulation of the activity of Crk and forms the basis of an autoinhibitory mechanism (*44*). Considering the internal motions near the acidic cluster and the structural difference between MEKK3 PB1 and MEKK2 PB1, the isomerization of Gln38−Pro39 bond and the back-end acidic cluster in MEKK3 PB1 may play a role in interactions with other potential partners. However, this possibility still needs to be elucidated.

ACKNOWLEDGMENT

We thank Dr. Yinshan Yang (INSERM, U554, Centre de Biochimie Structurale, 29, rue de Navacelles, F-34090 Montpellier, France) for excellent technical assistance in NMR experiments and Dr. Junjie Xu and Bo Yao for constructive advice in manuscript preparation. We also thank all the other members in our lab, past and present, who have contributed to this work. We thank Dr. F. Delaglio and Professor A. Bax for providing the software NMRPipe, Professors. T. D. Goddard and D. G. Kneller for providing Sparky, Professor A. T. Brünger for providing the program CNS, Dr. R. Koradi and Professor K. Wüthrich for providing MOLMOL, M. Carson for providing Ribbons, and Dr. W. L. DeLano for providing PyMOL.

SUPPORTING INFORMATION AVAILABLE

Gel-filtration chromatograms of MEK5, MEKK3, and their heterodimer; GST pull-down of GST-MEK5PB1 with MEKK3PB1; thermodynamic analysis of the MEKK3 PB1 mutants/MEK5 PB1 interaction by ITC; and HSQC spectrum of MEKK2 PB1. This material is available free of charge via the Internet at http://pubs.acs.org.

REFERENCES

1. Ravingerova, T., Barancik, M., and Strniskova, M. (2003) Mitogen-activated protein kinases: a new therapeutic target in cardiac pathology, *Mol. Cell. Biochem. 247*, 127−138.
2. Alessi, D. R., Cuenda, A., Cohen, P., Dudley, D. T., and Saltiel, A. R. (1995) PD 098059 is a specific inhibitor of the activation of mitogen-activated protein kinase kinase in vitro and in vivo, *J. Biol. Chem. 270*, 27489−27494.
3. Favata, M. F., Horiuchi, K. Y., Manos, E. J., Daulerio, A. J., Stradley, D. A., Feeser, W. S., Van Dyk, D. E., Pitts, W. J., Earl, R. A., Hobbs, F., Copeland, R. A., Magolda, R. L., Scherle, P. A., and Trzaskos, J. M. (1998) Identification of a novel inhibitor of mitogen-activated protein kinase kinase, *J. Biol. Chem. 273*, 18623−18632.
4. Johnson, G. L., Dohlman, H. G., and Graves, L. M. (2005) MAPK kinase kinases (MKKKs) as a target class for small-molecule inhibition to modulate signaling networks and gene expression, *Curr. Opin. Chem. Biol. 9*, 325−331.
5. Zhao, Q., and Lee, F. S. (1999) Mitogen-activated protein kinase/ERK kinase kinases 2 and 3 activate nuclear factor-κB through IκB kinase-α and IκB kinase-β, *J. Biol. Chem. 274*, 8355−8358.
6. Huang, Q., Yang, J., Lin, Y., Walker, C., Cheng, J., Liu, Z. G., and Su, B. (2004) Differential regulation of interleukin 1 receptor and Toll-like receptor signaling by MEKK3, *Nat. Immunol. 5*, 98−103.
7. Chao, T. H., Hayashi, M., Tapping, R. I., Kato, Y., and Lee, J. D. (1999) MEKK3 directly regulates MEK5 activity as part of the big mitogen-activated protein kinase 1 (BMK1) signaling pathway, *J. Biol. Chem. 274*, 36035−36038.
8. Nakamura, K., and Johnson, G. L. (2003) PB1 domains of MEKK2 and MEKK3 interact with the MEK5 PB1 domain for activation of the ERK5 pathway, *J. Biol. Chem. 278*, 36989−36992.
9. Gao, L., Joberty, G., and Macara, I. G. (2002) Assembly of epithelial tight junctions is negatively regulated by Par6, *Curr. Biol. 12*, 221−225.
10. Kuribayashi, F., Nunoi, H., Wakamatsu, K., Tsunawaki, S., Sato, K., Ito, T., and Sumimoto, H. (2002) The adaptor protein p40-(phox) as a positive regulator of the superoxide-producing phagocyte oxidase, *EMBO J. 21*, 6312−6320.
11. Betschinger, J., Mechtler, K., and Knoblich, J. A. (2003) The Par complex directs asymmetric cell division by phosphorylating the cytoskeletal protein Lgl, *Nature 422*, 326−330.
12. Cai, Y., Yu, F., Lin, S., Chia, W., and Yang, X. (2003) Apical complex genes control mitotic spindle geometry and relative size of daughter cells in *Drosophila* neuroblast and pI asymmetric divisions, *Cell 112*, 51−62.
13. Etienne-Manneville, S., and Hall, A. (2003) Cdc42 regulates GSK-3beta and adenomatous polyposis coli to control cell polarity, *Nature 421*, 753−756.
14. Hurd, T. W., Gao, L., Roh, M. H., Macara, I. G., and Margolis, B. (2003) Direct interaction of two polarity complexes implicated in epithelial tight junction assembly, *Nat. Cell Biol. 5*, 137−142.
15. Plant, P. J., Fawcett, J. P., Lin, D. C., Holdorf, A. D., Binns, K., Kulkarni, S., and Pawson, T. (2003) A polarity complex of mPar-6 and atypical PKC binds, phosphorylates and regulates mammalian Lgl, *Nat. Cell Biol. 5*, 301−308.
16. Hirano, Y., Yoshinaga, S., Takeya, R., Suzuki, N. N., Horiuchi, M., Kohjima, M., Sumimoto, H., and Inagaki, F. (2005) Structure of a cell polarity regulator, a complex between atypical PKC and Par6 PB1 domains, *J. Biol. Chem. 280*, 9653−9661.
17. Honbou, K., Minakami, R., Yuzawa, S., Takeya, R., Suzuki, N. N., Kamakura, S., Sumimoto, H., and Inagaki, F. (2007) Full-length p40phox structure suggests a basis for regulation mechanism of its membrane binding, *EMBO J. 26*, 1176−1186.
18. Iturrioz, X., and Parker, P. J. (2007) PKCzetaII is a target for degradation through the tumour suppressor protein pVHL, *FEBS Lett. 581*, 1397−1402.
19. Ito, T., Matsui, Y., Ago, T., Ota, K., and Sumimoto, H. (2001) Novel modular domain PB1 recognizes PC motif to mediate functional protein-protein interactions, *EMBO J. 20*, 3938−3946.
20. Moscat, J., Diaz-Meco, M. T., Albert, A., and Campuzano, S. (2006) Cell signaling and function organized by PB1 domain interactions, *Mol. Cell 23*, 631−640.
21. Nakamura, K., Uhlik, M. T., Johnson, N. L., Hahn, K. M., and Johnson, G. L. (2006) PB1 domain-dependent signaling complex is required for extracellular signal-regulated kinase 5 activation, *Mol. Cell. Biol. 26*, 2065−2079.
22. Nakamura, K., and Johnson, G. L. (2007) Noncanonical function of MEKK2 and MEK5 PB1 domains for coordinated extracellular signal-regulated kinase 5 and c-Jun N-terminal kinase signaling, *Mol. Cell. Biol. 27*, 4566−4577.

23. Cornilescu, G., Delaglio, F., and Bax, A. (1999) Protein backbone angle restraints from searching a database for chemical shift and sequence homology, *J. Biomol. NMR 13*, 289−302.
24. Wishart, D. S., and Sykes, B. D. (1994) The ^{13}C chemical-shift index: a simple method for the identification of protein secondary structure using ^{13}C chemical-shift data, *J. Biomol. NMR 4*, 171−180.
25. Koradi, R., Billeter, M., and Wuthrich, K. (1996) MOLMOL: a program for display and analysis of macromolecular structures, *J. Mol. Graphics 14*, 51−55.
26. Laskowski, R. A., Rullmann, J. A., MacArthur, M. W., Kaptein, R., and Thornton, J. M. (1996) AQUA and PROCHECK-NMR: programs for checking the quality of protein structures solved by NMR, *J. Biomol. NMR 8*, 477−486.
27. Farrow, N. A., Muhandiram, R., Singer, A. U., Pascal, S. M., Kay, C. M., Gish, G., Shoelson, S. E., Pawson, T., Forman-Kay, J. D., and Kay, L. E. (1994) Backbone dynamics of a free and phosphopeptide-complexed Src homology 2 domain studied by ^{15}N NMR relaxation, *Biochemistry 33*, 5984−6003.
28. Cole, R., and Loria, J. P. (2003) FAST-Modelfree: a program for rapid automated analysis of solution NMR spin-relaxation data, *J. Biomol. NMR 26*, 203−213.
29. Zhou, H., Xu, Y., Yang, Y., Huang, A., Wu, J., and Shi, Y. (2005) Solution structure of AF-6 PDZ domain and its interaction with the C-terminal peptides from Neurexin and Bcr, *J. Biol. Chem. 280*, 13841−13847.
30. Leavitt, S., and Freire, E. (2001) Direct measurement of protein binding energetics by isothermal titration calorimetry, *Curr. Opin. Struct. Biol. 11*, 560−566.
31. Liang, Y., Du, F., Sanglier, S., Zhou, B. R., Xia, Y., Van Dorsselaer, A., Maechling, C., Kilhoffer, M. C., and Haiech, J. (2003) Unfolding of rabbit muscle creatine kinase induced by acid. A study using electrospray ionization mass spectrometry, isothermal titration calorimetry, and fluorescence spectroscopy, *J. Biol. Chem. 278*, 30098−30105.
32. Schubert, M., Labudde, D., Oschkinat, H., and Schmieder, P. (2002) A software tool for the prediction of Xaa-Pro peptide bond conformations in proteins based on ^{13}C chemical shift statistics, *J. Biomol. NMR 24*, 149−154.
33. Thompson, J. D., Higgins, D. G., and Gibson, T. J. (1994) CLUSTAL W: improving the sensitivity of progressive multiple sequence alignment through sequence weighting, position-specific gap penalties and weight matrix choice, *Nucleic Acids Res 22*, 4673−4680.
34. Gouet, P., Courcelle, E., Stuart, D. I., and Metoz, F. (1999) ESPript: analysis of multiple sequence alignment in PostScript, *Bioinformatics 15*, 305−308.
35. Wilmot, C. M., and Thornton, J. M. (1988) Analysis and prediction of the different types of beta-turn in proteins, *J. Mol. Biol. 203*, 221−232.
36. Lipari, G., and Szabo, A. (1982) Model-free approach to the interpretation of nuclear magnetic resonance relaxation in macromolecules. 1. Theory and range of validity, *J. Am. Chem. Soc. 104*, 4546−4559.
37. Fisher, K. E., Ruan, B., Alexander, P. A., Wang, L., and Bryan, P. N. (2007) Mechanism of the kinetically-controlled folding reaction of subtilisin, *Biochemistry 46*, 640−651.
38. Brandts, J. F., Halvorson, H. R., and Brennan, M. (1975) Consideration of the possibility that the slow step in protein denaturation reactions is due to cis−trans isomerism of proline residues, *Biochemistry 14*, 4953−4963.
39. Wilson, M. I., Gill, D. J., Perisic, O., Quinn, M. T., and Williams, R. L. (2003) PB1 domain-mediated heterodimerization in NADPH oxidase and signaling complexes of atypical protein kinase C with Par6 and p62, *Mol. Cell 12*, 39−50.
40. Stewart, D. E., Sarkar, A., and Wampler, J. E. (1990) Occurrence and role of cis peptide bonds in protein structures, *J. Mol. Biol. 214*, 253−260.
41. Sumimoto, H., Kamakura, S., and Ito, T. (2007) Structure and function of the PB1 domain, a protein interaction module conserved in animals, fungi, amoebas, and plants, *Sci STKE 2007*, re6.
42. Santiveri, C. M., Perez-Canadillas, J. M., Vadivelu, M. K., Allen, M. D., Rutherford, T. J., Watkins, N. A., and Bycroft, M. (2004) NMR structure of the alpha-hemoglobin stabilizing protein: insights into conformational heterogeneity and binding, *J. Biol. Chem. 279*, 34963−34970.
43. Lummis, S. C., Beene, D. L., Lee, L. W., Lester, H. A., Broadhurst, R. W., and Dougherty, D. A. (2005) Cis-trans isomerization at a proline opens the pore of a neurotransmitter-gated ion channel, *Nature 438*, 248−252.
44. Sarkar, P., Reichman, C., Saleh, T., Birge, R. B., and Kalodimos, C. G. (2007) Proline cis-trans isomerization controls autoinhibition of a signaling protein, *Mol. Cell 25*, 413−426.

BI701341N